Symmetry-state features in a global analysis of the temperature-dependent spin transport in Fe/MgO/Fe junctions

C. Bellouard, Y. Lu, A. Duluard, B. Negulescu, Christian Senet, Nabila Maloufi, M. Hehn, C. Tiusan

Symmetry-state features in a global analysis of the temperature-dependent spin transport in Fe/MgO/Fe junctions

C. Bellouard,[1,*] Y. Lu,[1] A. Duluard,[1] B. Negulescu,[2] C. Senet,[1] N. Maloufi,[3] M. Hehn,[1] and C. Tiusan[4,5]

[1]*Institut Jean Lamour, CNRS-Université de Lorraine UMR 7198, Campus Artem, 2 allée André Guinier, 54011 Nancy, France*

[2]*Groupe de Recherche en Matériaux, Microélectronique, Acoustique et Nanotechnologies, UFR Sciences et techniques, Université de Tours, Parc de Grandmont, Bâtiment E, 37200, TOURS, France*

[3]*Université de Lorraine, Laboratoire d'Etude des Microstructures et de Mécanique des Matériaux LEM3, UMR 7239, F-57045 Metz Cedex 1, France*

[4]*Tech Univ Cluj Napoca, Ctr Superconduct, Spintron & Surface Sci, Str Memorandumului 28, RO-400114 Cluj Napoca, Romania*

[5]*Centre National de la Recherche Scientifique, DGDR, DR06, France*

(Received 18 July 2018; revised manuscript received 27 August 2018; published 26 October 2018)

The temperature dependence of the spin polarized tunnel conductance is investigated with Fe/MgO/Fe tunnel junctions with different structural properties and interfacial chemistry. A global quantitative model is proposed for analyzing the tunnel conductance in both parallel and antiparallel configuration. Three contributions to the temperature dependence can be distinguished. The first one is governed by the Bloch law for the temperature dependence of the magnetization of the electrodes. The second one is unpolarized and follows a power-law associated with a hopping mechanism. Although these two mechanisms are predominant in the decrease of tunnel magnetoresistance with temperature, a third contribution must be considered. This term results from a thermally activated decrease of the effective spin polarization, introduced by an Arrhenius law. It appears in either the parallel or antiparallel conductance, depending on the interface chemical doping, and could then be related to a symmetry dependent diffusion process. Finally, this global analysis appears universal, as it can well fit the temperature dependence of all samples.

DOI: 10.1103/PhysRevB.98.144437

I. INTRODUCTION

The prediction of an exceptional tunnel magnetoresistance (TMR) effect in FM/MgO/FM (FM: ferromagnetic) junctions has been the motivation for extensive experimental studies. Two different strategies were simultaneously developed: one using monocrystalline junctions grown on MgO (100) substrate which are expected to provide the best control of the structural parameters [1] and the second using textured junctions grown on Si wafers [2,3]. The optimization of the FM materials used as electrodes, of the growth and subsequent annealing conditions, led to a TMR ratio of several thousand percent at low temperature. These results made use of the properties of magnetic electrodes band structure, particularly with half-metallic electrodes [4,5]. Nevertheless, a much lower TMR ratio is measured at room temperature which remains limited to some hundred % whatever the spin-polarization properties of the ferromagnetic electrodes [5–10]. For a given MgO thickness, the decrease of the TMR with increasing temperature is in fact steeper in case of Heusler alloys than with conventional ferromagnetic electrodes [4,11]. The understanding of the temperature dependence is therefore a huge task to improve the TMR ratio at room temperature.

It is now well established that the decrease of TMR is mainly due to the steep increase of antiparallel (AP) conductance with temperature, whereas the parallel (P) conductance appears rather flat or even decreases in case of thin MgO barrier [5,6,8,9,12–22]. As a matter of fact, some authors proposed a model only considering the temperature dependence of the antiparallel conductance [8,23] or the TMR [6,7,18,24], disregarding the temperature dependence of the parallel conductance. Even among the studies considering the parallel conductance (or resistance), few papers present the fit of the experimental data on a relevant scale in order to exhibit its nonmonotonous dependence with temperature [5,19]. The parallel conductance, which exhibits a "quasi-flat" temperature dependence, appears indeed as a sensible parameter to test the theoretical models.

Based on the Jullière model [25], the TMR temperature dependence can be calculated assuming that the spin polarization follows a Bloch law [12]. This model provides opposite temperature dependence for the (P) and (AP) conductances, revealing a decrease (increase) of the parallel (antiparallel) conductance with temperature. This raw model was applied directly to the temperature dependence of the TMR [14], and of the conductance [16], but with different parameters in the Bloch law for (P) and (AP) configurations. In the case of a thin MgO barrier (typically <2 nm), the simple smearing factor describing the thermal energy broadening of the Fermi function appears sufficient to describe a non-monotonous temperature-dependent (P) conductance [19]. In the case of a thicker barrier, the increase of (P) and (AP) conductances with increasing temperature is enhanced and this model has to be improved. A spin independent term can be

*Author to whom correspondence should be addressed: christine.bellouard@univ-lorraine.fr

added with a power law temperature dependence describing a hopping mechanism [12,18,24]. Zhang *et al.* [26] proposed a spin flipping mechanism involving the inelastic tunneling thermally excited by magnons in the temperature dependence. It was consistently applied to thin CoFeB/MgO junctions [15]. However, a spin independent hopping term has to be added in the case of thick junctions [20,24]. The same model was applied to a MgO tunnel barrier with half metallic electrodes using a Bloch law temperature-dependent polarization, without any hopping mechanism. Nevertheless, different values of the parameters had to be introduced to fit the (P) and (AP) conductances [5]. Moreover, Lu *et al.* [17] have developed a model based on the extended Glazman-Matveev theory [27] with a mechanism of hopping assisted by spin-polarized tunneling. It appears more relevant for strongly temperature-dependent conductances or thick barrier [8,17] rather than for thinner ones where the direct tunneling mechanism has a larger contribution [20]. Finally, we point out that few studies include in the discussion the very specific symmetry filtering properties of MgO [17,28].

Up to now, the temperature dependence of the (P) and (AP) tunneling conductances remains under debate: a universal and global picture independent on the barrier thickness is still lacking. The present study proposes an analysis which can use consistent parameters to fit both the parallel and antiparallel conductances. Several types of Fe/MgO/Fe/Co junctions have been considered by tuning the structural (from textured to monocrystalline) and interface chemical properties (carbon doping). The introduction of a phenomenological term is discussed in terms of the wave functions' symmetry impact on the temperature dependence of the tunneling conductances.

II. EXPERIMENTAL DETAILS

This paper gathers results obtained from four different junctions. They are all grown by ultrahigh vacuum molecular beam epitaxy (MBE) equipped with reflection high-energy electron diffraction (RHEED). The magnetic electrodes consist of a thick (from 30 to 60 nm) soft Fe layer first deposited on the substrate, and of a hard Fe/Co bilayer deposited after the MgO tunnel barrier. The thickness of the MgO barrier is controlled with RHEED intensity oscillations. Finally, the structure is capped with an Au layer to prevent oxidation.

The first two junctions, denoted as M1 and M1C, have a monocrystalline structure and are grown on the same wafer, as reported in Ref. [28]. The multilayer structures are MgO(100) substrate/alternative MgO (3 nm)/ Fe(45 nm)/MgO (12 ML)/ Fe (10 nm)/Co(20 nm)/Au(10 nm), where ML stands for monolayer. With the use of an *in situ* shutter, the alternative 3-nm MgO layer is present only in the M1 stack where it serves as an antidiffusion layer for the carbon in the substrate. Due to the absence of this antidiffusion layer in the M1C stack, M1C is doped by carbon at the bottom Fe/MgO interface with an ordered $c2 \times 2$ reconstruction after the annealing of the bottom Fe layer at 450 °C (for 30 min) [28–30]. The Fe top layer is annealed at 350 °C for 20 min.

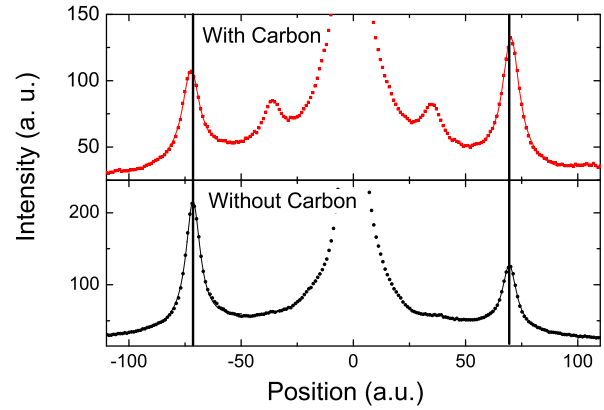

FIG. 1. RHEED intensity profile in the Fe [110] azimuth. The surface with carbon shows a 2×2 reconstruction. The solid lines are fits with a Lorentzian law with a linear background.

Figure 1 shows RHEED intensity profiles of a Fe bottom layer after annealing. The ordered carbon-doped Fe/MgO interface exhibits the well-known 2×2 reconstruction. Moreover the diffraction lines (marked with black lines) characterizing the surface lattice parameter are slightly distant, indicating a contraction of the surface lattice. Thanks to a fit with a Lorentzian law performed with several samples, the shift can be evaluated to about 1%. As a matter of fact, the presence of carbon enhances the lattice mismatch of 3.7% between the bulk lattice parameters of Fe and MgO.

The third junction presented in this paper and referred to as "T" is deposited on a (100) Si substrate coated with a 5-nm-thick MgO film in a separate sputtering chamber. The magnetic tunnel junction composed of Fe 30 nm/MgO(11.5ML)/ Fe 10 nm/Co 20 nm/Au 20 nm is then grown by molecular beam epitaxy as described in Ref. [22]. It has been shown that subsequent annealing of the ferromagnetic Fe layers (at 500 °C, 20 min and 350 °C, 10 min for bottom and top respectively), checked by *in situ* RHEED, provides highly (100) textured electrodes [22]. A "grain to grain" epitaxy is then achieved resulting in a so-called "fiber textured" junction. Nevertheless, the *in situ* RHEED intensity oscillations observed during the deposition of the MgO barrier exhibits a

TABLE I. Main characteristics of the junctions: the monocrystalline junctions grown on MgO substrate are called M1 and M2. M1C designates a monocrystalline junction with carbon at the interface. T designates a fiber textured junction. The thickness of the MgO tunnel barrier is indicated in monolayers (ML).

Samples	Substrate	Deposited stack	TMR (10 K) 10 mV	TMR (10 K) −1V
M1	MgO(100)	MgO/Fe/MgO (12 ML)/Fe/Co	290%	48%
M1C	MgO(100)	Fe(FeC)/MgO (12 ML)/Fe/Co	288%	−57%
T	Si(100)	MgO sputt. / Fe/MgO (11.5 ML)/Fe/Co	170%	
M2	MgO(100)	MgO/Fe/MgO (10 ML)/Fe/Co	165%	

faster damping than in the case of monocrystalline junctions [22], indicating a less flat MgO surface. The average lateral grain size estimated from the in-plane x-ray diffraction is about 25 nm [22].

Finally, we also report the results of a monocrystalline junction denoted as M2, grown by MBE on a MgO (100) substrate, whose top electrode was not annealed after growth. The whole deposited stack is: MgO(10 nm) /Fe(60 nm)/MgO (10 ML)/Fe(13 nm)/Co(30 nm)/Au(10 nm). The bottom Fe electrode was annealed at 500 °C (30 min) as for the other junctions (M1, M1C, T). Details of the growth conditions can be found in Ref. [31]. Table I gathers the main features of the different junctions.

The magnetotransport measurements were performed with a two-probe DC configuration. The negative bias corresponds to the electron tunneling from the top electrode to the bottom electrode.

III. RESULTS AND DISCUSSION

Figure 2 show the zero bias (10 mV) temperature dependence of the tunneling magnetoresistance [Fig. 2(a)] and the normalized TMR [Fig. 2(b)]. The carbon contaminated junction clearly exhibits a stronger decrease of TMR of about 60% from 10 to 300 K, whereas the decrease of the other junctions is about 40–45%. As already mentioned, this decrease of TMR is mainly governed by the increase of the antiparallel conductance with temperature, and the parallel conductance varies little with temperature, as discussed below.

Figure 3 presents the relative temperature dependence of the parallel and antiparallel conductances, presented per area unit (G/A). M1, T, and M2 show qualitatively similar features, with a nonmonotonic dependence of the parallel conductance, whereas the antiparallel one presents a strong increase with

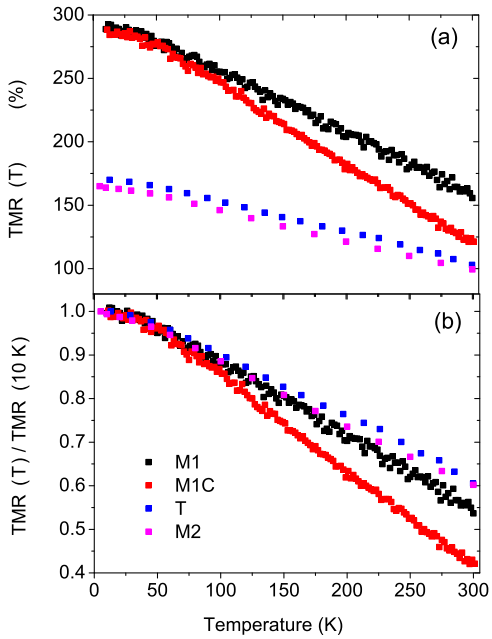

FIG. 2. Temperature dependence of the tunneling magnetoresistance measured (a) at 10 mV and (b) normalized to its low temperature value.

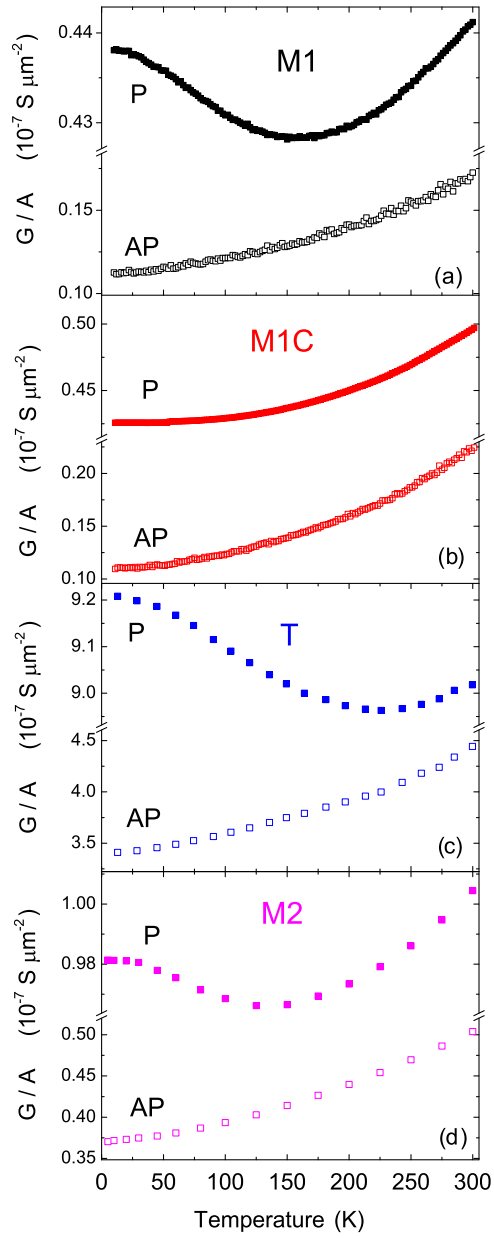

FIG. 3. Temperature dependence of parallel (P) and antiparallel (AP) conductances (per area unit) measured at 10 mV for junctions (a) M1, (b) M1C, (c) T, and (d) M2.

temperature (note the different scales for parallel and antiparallel conductances). According to the simple model of elastic tunneling derived by Shang *et al.* [12] from the Jullière model, the parallel and antiparallel conductances would follow opposite temperature dependences written as

$$G_P(T) = G_0 \frac{CT}{\sin(CT)} [1 + P^2 (1 - \alpha T^{3/2})^2], \quad (1)$$

$$G_{AP}(T) = G_0 \frac{CT}{\sin(CT)} [1 - P^2 (1 - \alpha T^{3/2})^2], \quad (2)$$

where G_0 is a constant. The temperature dependence is due to the smearing factor: $CT/\sin(CT)$ (broadening of the Fermi distribution), with $C = 1.387 \times 10^{-4}\, d/\sqrt{\varphi}$ where d is the

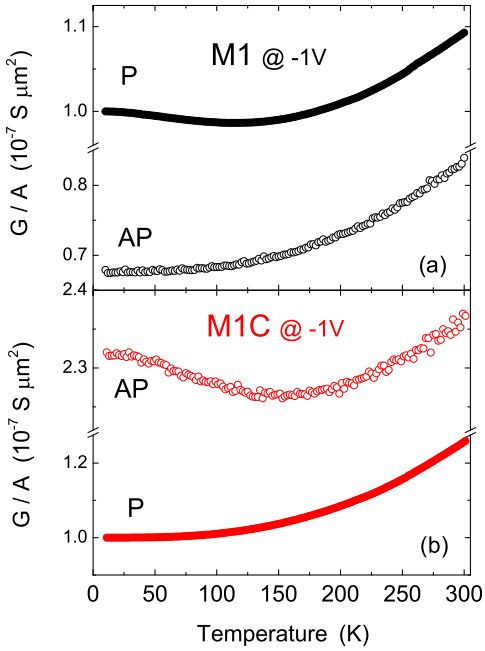

FIG. 4. Temperature dependence of parallel and antiparallel conductances (per area unit) measured at −1 V for (a) M1, and (b) M1C junctions.

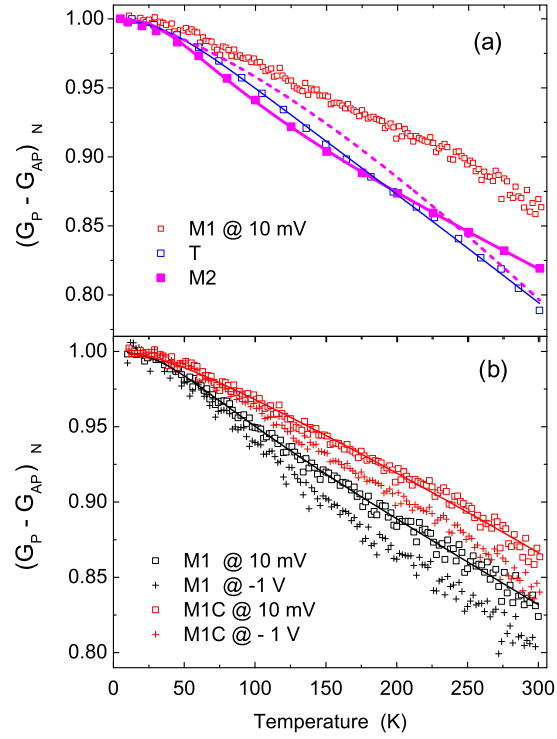

FIG. 5. Difference between parallel and antiparallel conductances normalized to its value at 10K; (a) M1, T, and M2 at 10 mV. (b) M1 and M1C at 10 mV and −1 V. The dashed line in (a) is a fit for the M2 junction with Eq. (4). The straight lines in (a) and (b) are fits according to Eq. (5).

barrier width in Å, and φ is the barrier height in eV [32]. The temperature dependence of the spin polarization is described by a Bloch law, α is a material-dependent constant. "P" is the spin-polarization of the junction at $T = 0$ K which can be deduced from the TMR at 0 K as

$$\mathrm{TMR}(T = 0\,\mathrm{K}) = 2\mathrm{P}^2/(1 - \mathrm{P}^2) \tag{3}$$

This basic model provides a decrease of $G_P(T)$ and an increase of $G_{AP}(T)$ with temperature. As shown in Fig. 3, it is indeed observed at the low temperature range, below roughly 100 K, for all junctions, except M1C.

The carbon contaminated junction M1C has a peculiar behavior, as illustrated also in Fig. 4(b) for −1V bias. Under such a bias, as shown in our previous work [28,30], because of the contribution of an interfacial resonance state (IRS) in the minority channel dominated by the Δ_1 symmetry, G_{AP} can exceed G_P, and the TMR becomes negative. Interestingly, in that configuration, the temperature dependence of the conductances in the carbon contaminated junction recovers a behavior similar to the carbon free junction under low bias [presented in Fig. 4(a)]. The dominant conductance G_{AP} (M1C), enhanced by the IRS Δ_1 symmetry channel, exhibits a nonmonotonous behavior, as G_P for undoped junctions, whereas G_P (M1C) increases with temperature as G_{AP} for other junctions. The low temperature behavior of the carbon-doped junction at −1V can then be described by Eqs. (1) and (2) with $\mathrm{P}^2 < 0$, because of $G_{AP} > G_P$. In contrast, the behavior of the undoped junction at −1V bias [Fig. 4(a)] is qualitatively similar to the case under low bias [Fig. 3(a)].

On the contrary, at temperatures above roughly 100 K, the conductances increase with temperature, in both (P) and (AP) states for all type of junctions. Then, it seems reasonable to consider a third contribution to the temperature dependence, related to a thermally activated conduction mechanism. This additional channel is superimposed to the other conduction channels, whatever is their polarization state. This third contribution is then assumed to be spin independent. Therefore, its contribution should be canceled out when considering the difference $G_P(T) - G_{AP}(T)$.

The difference $G_P - G_{AP}$ normalized to its low temperature value, $(G_P - G_{AP})_N = (G_P - G_{AP})(T)/(G_P - G_{AP})(10\,\mathrm{K})$, is plotted in Figs. 5(a) and 5(b). Interestingly, for all junctions and applied bias, despite very different temperature behavior of the conductances, this scaling procedure provides a common temperature variation, $(G_P - G_{AP})_N$, which closely decreases from 12 to 20% with increasing temperature.

The qualitative behavior of $(G_P - G_{AP})_N$ is then consistent with its expression deduced from Eqs. (1) and (2):

$$(G_p - G_{AP})_N\,(T) = \frac{CT}{\sin(CT)}\,(1 - \alpha\,T^{3/2})^2. \tag{4}$$

The decrease with temperature can be then described mainly by the Bloch law. The smearing factor C increases with temperature but is only a few percent higher at 300 K than at $T = 0$ K [5,12] for typical d and φ values. As a matter of fact, in previous studies, the smearing factor was neglected [16] or fixed [5,12,17]. In the following treatments, φ is fixed to a value of 3.9 eV, corresponding to half of the experimental gap (7.8 eV) of the MgO barrier [33,34] and "d" is given by the known value of barrier thickness (deduced from RHEED intensity oscillations during growth).

TABLE II. Parameters fixed (C*) or deduced from the fit of normalized $(G_P - G_{AP})$ with Eq. (5). The uncertainty is the standard error provided by the fitting software, it has then to be multiplied by 2 to get a 95% confidence level.

Samples	C*(10^{-3} K^{-1})	α(10^{-5} K$^{-3/2}$)	A_{P-AP}($\times 10^{-2}$)	E (K)
M1	1.75	1.59 ± 0.05	8.6 ± 0.9	129 ± 7
M1C	1.75	1.60 ± 0.05	3 ± 1	163 ± 30
T	1.70	2.06 ± 0.09	8 ± 2	173 ± 18
M2	1.48	1.33 ± 0.05	13.3 ± 0.5	123 ± 5

Figure 5(a) shows an attempt of fitting with Eq. (4) for junction M2 (pink dashed line), the deviation with the experimental data is clear and an additional factor corresponding to a thermally activated loss of conductance has to be considered. A simple Arrhenius law, introduced in Eq. (5), is indeed enough to get a satisfactory fit as shown by the straight lines in Figs. 5(a) and 5(b).

$$(G_p - G_{AP})_N\,(T) = \frac{CT}{\sin(CT)}\,(1-\alpha\,T^{3/2})^2 \times \left(1 - A_{P-AP}\,\exp\left(-\frac{E}{T}\right)\right). \quad (5)$$

The parameters fixed or obtained from the fitting of $(G_P - G_{AP})_N$ at low bias are reported in Table II.

The physical meaning of the Arrhenius law will be discussed later. No physical meaning can be attributed at this stage to A_{P-AP} which can stand for a decrease of G_P, an increase of G_{AP}, or both. All the α values are larger than that measured by temperature-dependent magnetization ($\approx 3 \times 10^{-6}$ K$^{-3/2}$). Such behavior has been already reported and attributed to an interface contribution mainly probed in the TMR study [12,14]. Interestingly, the same value of α is provided by the fit for M1 and M1C, which have identical magnetic electrodes but exhibit very different temperature dependence of their conductances. This result further supports the present analysis and the relevance of the Arrhenius law in Eq. (5).

The spin dependent term of the conductances can then be taken into account in the frame of the Jullière model by introducing an Arrhenius law, with amplitude A_P and A_{AP} for parallel and antiparallel conductances, associated to the Bloch law as written in Eqs. (6) and (7).

The increase of the spin independent term with temperature, observed in both conductances, suggests a power law dependence as found in the case of the hopping mechanism assisted by defects. The exponent γ is then related to the number N of localized states in the barrier through $\gamma(N) = N - (2/(N+1))$, which provides $\gamma(2) = 4/3$ and $\gamma(3) = 5/2$ [27]. This power law, first used for the semiconducting barrier, has also been used to describe a spin independent term in case of insulating barrier as Al_2O_3 [12] or MgO [24,20] or an extended spin dependent term [17]. We note that $N = 1$ corresponds to a flat temperature dependence which is readily taken into account in the effective polarization P.

The normalized conductances with respect to their respective low temperature values, $G_{P(AP)-N}(T) = \frac{G_{P(AP)}(T)}{G_{P(AP)}(10\,\mathrm{K})}$, can be fitted with the following equations:

$$G_{P-N}(T) = \frac{1}{1+P^2}\left[1 + P^2(1-\alpha T^{3/2})^2 \times \left(1 - A_P\,\exp\left(-\frac{E}{T}\right)\right)\right]\frac{CT}{\sin(CT)} + SI, \quad (6)$$

$$G_{AP-N}(T) = \frac{1}{1-P^2}\left[1 - P^2(1-\alpha T^{3/2})^2 \times \left(1 - A_{AP}\exp\left(-\frac{E}{T}\right)\right)\right]\frac{CT}{\sin(CT)} + \frac{1+P^2}{1-P^2}SI, \quad (7)$$

$$SI = H_2\,T^{4/3} + H_3\,T^{5/2}. \quad (8)$$

A_P and A_{AP} are the amplitude of the Arrhenius law, H_2 and H_3 are, respectively, the weight of the $N = 2$ and $N = 3$ hopping terms in the normalized parallel conductance.

We point out that only one parameter differs between $G_{P-N}(T)$ and $G_{AP-N}(T)$: the amplitude of the Arrhenius law, A_P and A_{AP}. These parameters are related to A_{P-AP} in Eq. (5) by

$$A_{P-AP} = \frac{A_P + A_{AP}}{2}. \quad (9)$$

The Arrhenius law of Eqs. (6) and (7) describes a thermally activated decrease of polarization. In a classical Jullière approach, A_P should be equal to A_{AP}. Here, because of the specific features of transport properties in the Fe/MgO system, due to symmetry filtering or electronic state density, a decrease of the effective polarization in the parallel conductance is not necessarily balanced by the same effect in the antiparallel conductance, as will be discussed below.

For each curve, there are five parameters to fit: α, A_P (A_{AP}), E, H_2 and H_3. In order to get reasonable values, α has been fixed to its value reported in Table II. For junctions M1, T, and M2 which exhibit a nonmonotonous temperature dependence of $G_{P-N}(T)$, it was possible to fit A_P,E, H_2 and H_3 with G_{P-N} [Fig. 6(a)]. These values have then been fixed to fit $G_{AP-N}(T)$ by varying only one parameter A_{AP}. Surprisingly, it can provide satisfactory fits as illustrated in Fig. 6(b).

For the carbon doped junction M1C, the fit of $G_{P-N}(T)$ with variable A_P, E, H_2, and H_3 provides $E = 215$ K, with a standard deviation of 50 K. This value is in agreement with Table II, but with a large uncertainty (100 K). The value of E has then been fixed to the value obtained with $(G_P - G_{AP})_N$, and the other parameters have been fitted as for the other junctions [Figs. 6(c) and 6(d)].

The fitted curves are represented by straight lines in Figs. 6(a)–6(d). The values of the fixed or fitted parameters are listed in Table III.

For the M1 and M2 junctions, the activation energies "E" reported in Table III agree also with those of Table II; taking into account the uncertainties. The A_P and A_{AP} values

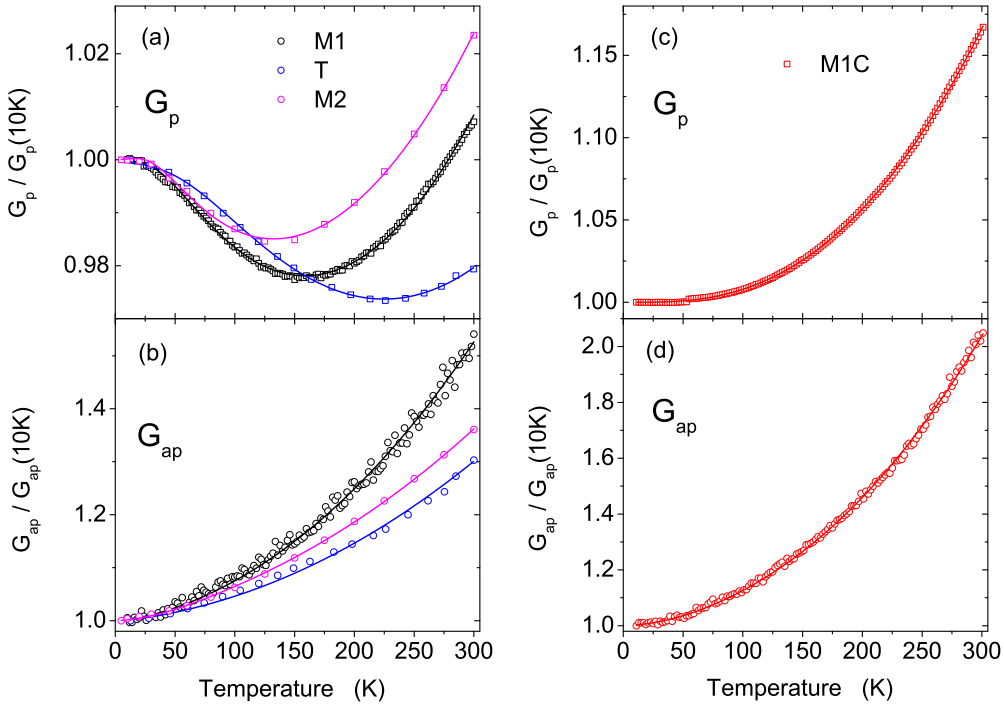

FIG. 6. (a) and (b) normalized parallel and antiparallel conductances measured at 10 mV for M1, T, and M2 junctions and fitted with Eqs. (6) and (7), the straight lines corresponds to the fits; (c) and (d) Normalized parallel and antiparallel conductances measured at 10 mV for M1C junction and fitted with Eqs. (6) and (7), the straight lines correspond to the fits.

reported in Table III are also in perfect agreement with A_{P-AP} of Table II according to Eq. (9) for M1, M1C, and M2 junctions. These results insure that the spin independent part is then finely shaped by the power laws.

Concerning the "T" junction, the interval values of the activation energy with a 95% confidence level are close in the two tables: 245 K ± 16 K (Table III) and 173 K ± 36 K (Table II). The values of $(A_P + A_{AP})/2$ are also close: 0.08 ± 0.04 (Table II) with respect to 0.12 ± 0.01 (Table III). As a matter of fact, in that case, the spin independent term may deviate from the power law, and this could be related to the specific textured structure. Anyway, we can consider that the main contribution to the spin independent term has been extracted from the experimental results.

A_P and A_{AP} are both positive or null for M1, M1C, and M2, which agree with a decrease of the effective polarization by a thermal activated process. The negative value of A_{AP} for the "T" junction which has a much smaller absolute value than A_P has no physical meaning. In fact, if we consider a MgO thickness of 10.5 ML instead of 11.5 ML, we can get a positive value close to zero for this sample. Therefore, the following discussion only concerns the trends of the fitted parameters.

The main contribution of the thermally activated term concerns the parallel conductance for M1, T, and M2 samples. A_P is responsible for the decrease of the order of 20% of the effective polarization. However, the corresponding relative decrease of polarization seen in the antiparallel conductance is much smaller or negligible. Since the parallel conductance is mainly dominated by the Δ_1 symmetry, which is expected to be almost absent in G_{AP}, it is quite obvious to associate this term with a scattering process to the Δ_1 Bloch state. Any inelastic diffusion process of the Δ_1 symmetry state towards other symmetries such as Δ_1 or Δ_5 states would indeed induce a decrease of effective tunneling polarization because the latter symmetry channels have lower polarization. This tunneling polarization is indeed not only the electrode polarization, but it reflects also the tunneling transmission probability of the spin-polarized state. The symmetry dependent transmission

TABLE III. Parameters fixed or deduced from the fit of the normalized parallel and antiparallel conductances at 10 mV by Eqs. (6) and (7), respectively. The uncertainties are the standard error provided by the fit. The parameters which have been fixed during a fit are noted with an asterisk (*).

Samples	α* (10^{-5} K$^{-3/2}$)	P*	E (K)	A_P ($\times 10^{-2}$)	A_{AP} ($\times 10^{-2}$)	H_2 (10^{-6} K$^{-4/3}$)	H_3 (10^{-8} K$^{-5/2}$)	$(A_P + A_{AP})/2$ ($\times 10^{-2}$)
M1	1.59	0.769	145 ± 1.5	18.6 ± 0.5	0.3 ± 0.2	6.1 ± 1.2	3.1 ± 0.1	9.5 ± 0.3
M1C	1.60	0.768	163*	1.6 ± 0.5	5.1 ± 0.2	11.7 ± 0.8	10.3 ± 0.05	3.3 ± 0.3
T	2.06	0.677	245 ± 8	27 ± 1	−2.6 ± 0.7	3.5 ± 1.3	1.6 ± 0.1	12.2 ± 0.6
M2	1.33	0.672	120 ± 3	21 ± 2	5.1 ± 0.1	16 ± 3	2.5 ± 0.3	13.0 ± 1

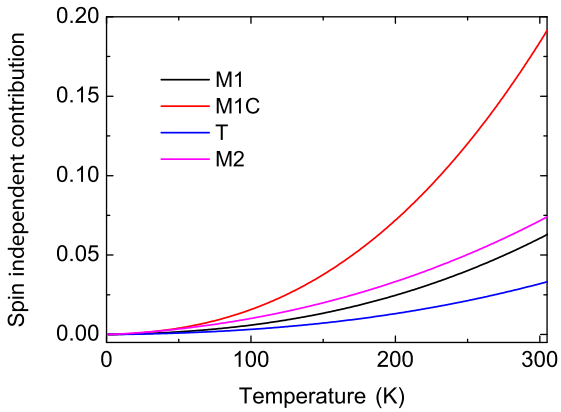

FIG. 7. Spin independent contribution to the normalized parallel conductance deduced from the fitted parameters H_2 and H_3.

across the single crystal MgO, which is lower for the other symmetry (Δ_2 or Δ_5), takes a part in the decrease of effective polarization.

Interestingly, the M1C junction exhibits a completely different behavior: the weight of the Arrhenius term is much lower ($\simeq$5% of the polarization) and the major relative contribution concerns the antiparallel conductance. This feature is reminiscent of the negative bias effect: with applied negative voltage, the antiparallel conductance increases and even exceeds the parallel conductance, resulting in a decrease of polarization which even becomes negative. This feature has been well understood with the contribution of the interfacial resonance surface state [28–30]. The peculiar nature of the carbon doped interface lies in the enhancement of the interfacial resonance state with Δ_1 dominant character in the minority band, which opens a conduction channel in the antiparallel configuration. As a matter of fact, a diffusion process of the Δ_1 symmetry state could also be responsible for the Arrhenius term behavior of the carbon doped junction.

The activation energy "E", in the range 10–20 meV, is of the order of the phonon excitations. An electron-phonon scattering could be responsible for the diffusion process described by the Arrhenius term. Depending on the symmetry potential, such inelastic scattering can indeed modify the symmetry of the wave function. The fact that carbon doping tends to quench this process could be related to the additional strain induced by carbon in the MgO barrier, as observed with RHEED patterns (Fig. 1). Carbon atoms could enhance the cohesion between atoms at the interface, and then restrict the possibility of phonons excitations. It could also be correlated to the strong reduction of $1/f$ noise observed in carbon doped junctions with a 12-ML MgO barrier [35].

Figure 7 shows the temperature dependence of the spin independent term SI [Eq. (8)] of the four junctions. Interestingly, it is the textured junction which has the lowest temperature dependence, whereas the strongest temperature dependence is observed with the carbon doped interface. This behavior can be attributed to extended defects inside the barrier (i.e., dislocations) [8]. As the surface lattice mismatch between Fe and MgO is enhanced by the carbon interface doping, a larger dislocation density is expected in the barrier as well as a stronger contribution of hopping in the conductance [8]. The textured junction that allows the strains relaxing at grains boundaries may have a better crystalline structure inside the grain, owing to the so-called "grain to grain epitaxy" [22,36].

Finally, using the fitted parameters presented in Table III, the weight of the three contributions (Bloch law, Arrhenius law, and spin independent term) in the TMR decrease between 10 and 300 K can be evaluated. It is found that, for all samples, the temperature dependence of TMR is essentially governed by the interface magnetic disorder (Bloch law). The second factor which weighs the decrease of TMR with increasing temperature is the spin independent term associated with the tunnel barrier defects such as dislocations. The strongest contribution from this factor is found for the M1C junction where it is responsible for almost 40% of the decrease of TMR. Both of these contributions have been tuned with different structural parameters through the M1, M2, and T junctions. Nevertheless, the "M2" junction which has the lowest α value has the strongest $SI(T)$ dependence, whereas the "T" junction has the lowest $SI(T)$ dependence and the highest α value. Because of this balance effect, the three junctions have very similar TMR(T) dependence (Fig. 2).

IV. CONCLUSION

A global phenomenological analysis of magnetization-dependent conductances has been carried out using several Fe/MgO epitaxial junctions with tuning chemical/structural properties. The analysis of the spin dependent component of the conductances is based on the Jullière model, assuming an effective polarization at low temperature. Two mechanisms are then responsible for the decrease of the effective polarization with temperature: the decrease of magnetization of the electrodes (Bloch law) and a thermally activated process strongly dependent on the chemical properties of the junction interface, which is known to tune the electronic Bloch state symmetry of the tunneling electrons. It is therefore associated with a diffusion process towards a less polarized Bloch state, which could be induced by phonons scattering. The analysis of the spin independent term is based on a power law, in the frame of hopping mechanisms. This model consistently fits both monotonous or nonmonotonous (P) and (AP) conductances versus temperature with only one different parameter. The puzzling increase of parallel conductance at high temperature is then attributed to the spin independent term. Finally, the temperature dependence of the interfacial magnetization of the ferromagnetic electrode is found to be the main contribution to the TMR decrease with increasing temperature.

ACKNOWLEDGMENTS

This work was supported by the French PIA project "Lorraine Université d'Excellence", reference ANR-15-IDEX-04-LUE. Y.L. acknowledges the support of the joint French National Research Agency (ANR)-National Natural Science Foundation of China (NSFC) ENSEMBLE Project (Grants No. ANR-14-0028-01 and No. NNSFC 61411136001). C.T. acknowledges "EMERSPIN" Grants No. ID PN-III-P4-ID-PCE-2016-0143 from UEFISCDI agency No. 22/12.07.2017.

[1] S. Yuasa, T. Nagahama, A. Fukushima, Y. Suzuki, and K. Ando, Nat. Mater. **3**, 868 (2004).

[2] S. S. P. Parkin, C. Kaiser, A. Panchula, P. M. Rice, B. Hughes, M. Samant, and S.-H. Yang, Nat. Mater. **3**, 862 (2004).

[3] S. Ikeda, J. Hayakawa, Y. Ashizawa, Y. Lee, K. Miura, H. Hasegawa, M. Tsunoda, F. Matsukura, and H. Ohno, Appl. Phys. Lett. **93**, 082508 (2008).

[4] S. Tsunegi, Y. Sakuraba, M. Oogane, N. D. Telling, L. R. Shelford, E. Arenholz, G. van der Laan, R. J. Hicken, K. Takanashi, and Y. Ando, J. Phys. D: Appl. Phys. **42**, 195004 (2009).

[5] B. Hu, K. Moges, Y. Honda, H. X. Liu, T. Uemura, M. Yamamoto, J. Inoue, and M. Shirai, Phys. Rev. B **94**, 094428 (2016).

[6] Z. Wen, H. Sukegawa, S. Mitani, and K. Inomata, Appl. Phys. Lett. **98**, 192505 (2011).

[7] M. A. Tanaka, T. Hori, K. Mibu, K. Kondou, T. Ono, S. Kasai, T. Asaka, and J. Inoue, J. Appl. Phys. **110**, 073905 (2011).

[8] M. S. Gabor, C. Tiusan, T. Petrisor Jr., T. Petrisor, M. Hehn, Y. Lu, and E. Snoeck, J. Magn. Magn. Mater. **347**, 79 (2013).

[9] M. A. Tanaka, D. Maezaki, T. Ishii, A. Okubo, R. Hiramatsu, T. Ono, and K. Mibu, J. Appl. Phys. **116**, 163902 (2014).

[10] L. Bainsla, K. Z. Suzuki, M. Tsujikawa, H. Tsuchiura, M. Shirai, and S. Mizukami, Appl. Phys. Lett. **112**, 052403 (2018).

[11] G.-f. Li, Y. Honda, H.-x Liu, K. I. Matsuda, M. Arita, T. Uemura, M. Yamamoto, Y. Miura, M. Shirai, T. Saito, F. Shi, and P. M. Voyles, Phys. Rev. B **89**, 014428 (2014).

[12] C. H. Shang, J. Nowak, R. Jansen, and J. S. Moodera, Phys. Rev. B. **58**, R2917(R) (1998).

[13] G.-X. Miao, K. B. Chetry, A. Gupta, W. H. Butler, K. Tsunekawa, D. Djayaprawira, and G. Xiao, J. Appl. Phys. **99**, 08T305 (2006).

[14] S. G. Wang, R. C. C. Ward, G. X. Du, X. F. Han, C. Wang, and A. Kohn, Phys. Rev. B **78**, 180411(R) (2008).

[15] V. Drewello, J. Schmalhorst, A. Thomas, and G. Reiss, Phys. Rev. B **77**, 014440 (2008).

[16] Q. L. Ma, S. G. Wang, J. Zhang, Y. Wang, R. C. C. Ward, C. Wang, A. Kohn, X.-G. Zhang, and X. F. Han, Appl. Phys. Lett. **95**, 052506 (2009).

[17] Y. Lu, M. Tran, H. Jaffrès, P. Seneor, C. Deranlot, F. Petroff, J.-M. George, B. Lépine, S. Ababou, and G. Jézéquel, Phys. Rev. Lett. **102**, 176801 (2009).

[18] R. Matsumoto, A. Fukushima, K. Yakushiji, S. Nishioka, T. Nagahama, T. Katayama, Y. Suzuki, K. Ando, and S. Yuasa, Phys. Rev B **79**, 174436 (2009).

[19] J. M. Teixeira, J. Ventura, J. P. Araujo, J. B. Sousa, P. Wisniowski, and P. P. Freitas, Appl. Phys. Lett. **96**, 262506 (2010).

[20] A. A. Kahn, J. Schmalhorst, G. Reiss, G. Eilers, M. Münzenberg, H. Schuhmann, and M. Seibt. Phys. Rev. B **82**, 064416 (2010).

[21] Z. Kugler, V. Drewello, M. Schäfers, J. Schmalhorst, G. Reiss, and A. Thomas. J. Magn. Magn. Mater. **323**, 198 (2011)

[22] A. Duluard, B. Negulescu, C. Bellouard, M. Hehn, D. Lacour, Y. Lu, G. Lengaigne, F. Montaigne, S. Robert, S. Suire, and C. Tiusan, Appl. Phys. Lett. **100**, 072408 (2012).

[23] X.-G. Zhang, Yan Wang, and X. F. Han. Phys. Rev. B **77**, 144431 (2008).

[24] X. Kou, J. Schmalhorst, A. Thomas, and G. Reiss, Appl. Phys. Lett. **88**, 212115 (2006).

[25] M. Julliere, Phys. Lett. A **54**, 225 (1975).

[26] S. Zhang, P. M. Levy, A. C. Marley, and S. S. P. Parkin. Phys. Rev. Lett. **79**, 3744 (1997).

[27] L. I. Glazman and K. A. Matveev, Zh. Eksp. Teor. Fiz. **94**, 332 (1988).

[28] Y. Lu, H.-X. Yang, C. Tiusan, M. Hehn, M. Chshiev, A. Duluard, B. Kierren, G. Lengaigne, D. Lacour, C. Bellouard, and F. Montaigne, Phys. Rev. B **86**, 184420 (2012).

[29] C. Tiusan, M. Sicot, M. Hehn, C. Belouard, S. Andrieu, F. Montaigne, and A. Schuhl, J. Appl. Phys. Lett. **88**, 062512 (2006).

[30] C. Tiusan, F. Greullet, M. Hehn, F. Montaigne, S. Andrieu, and A. Schuhl, J. Phys.: Condens. Matter **19**, 165201 (2007).

[31] A. Duluard, C. Bellouard, Y. Lu, M. Hehn, D. Lacour, F. Montaigne, G. Langaigne, S. Andrieu, F. Bonell, and C. Tiusan, Phys. Rev. B **91**, 174403 (2015).

[32] R. Stratton, J. Phys. Chem. Solids **23**, 1177 (1962).

[33] M. Kurth, P. C. J. Graat, and E. J Mittemeijer, Thin Solid Films **500**, 61 (2006).

[34] S. Heo, E. Cho, H.-I. Lee, G. Su Park, H. Jae Kang, T. Nagatomi, P. Choi, and B.-D. Choi, AIP Adv. **5**, 077167 (2015).

[35] D. Herranz, R. Guerrero, J. P. Cascales, F. G. Aliev, M. Hehn, and C. Tiusan, Acta Phys. Pol. A, **121**, 981 (2012).

[36] Y. S. Choi, T. Tsunekawa, Y. Nagamine, and D. Djayaprawira, J. Appl. Phys. **101**, 013907 (2007).